

# Extraplanar Dust in the Edge-On Spiral NGC 891<sup>1</sup>

J. Christopher Howk<sup>2</sup> & Blair D. Savage<sup>3</sup>

Department of Astronomy, University of Wisconsin-Madison  
Madison, Wi. 53706

## ABSTRACT

We present high-resolution (0.6''-0.65'') optical broad-band images of the edge-on Sb galaxy NGC 891 obtained with the WIYN 3.5-m telescope. These BVR images reveal a complex network of hundreds of dust absorbing structures far from the mid-plane of the galaxy. The dust structures have a wide range of morphologies and are clearly visible to  $|z| \lesssim 1.5$  kpc from the mid-plane. In this paper we discuss the general characteristics of the population of absorbing structures, as well as physical properties of 12 individual features. These 12 structures are characterised by  $N_H \gtrsim 10^{21} \text{ cm}^{-2}$ , with masses estimated to be more than  $2 \times 10^5 - 5 \times 10^6 M_\odot$ , assuming Galactic gas-to-dust relationships. The gravitational potential energies of the individual dust structures, given their observed heights and derived masses, lie in the range of  $20 - 200 \times 10^{51}$  ergs, which represents the energy input of at least tens to hundreds of supernovae. Rough number counts of extraplanar dust features find  $\gtrsim 120$  structures at  $|z| > 400$  pc with apparent B-band extinction  $\gtrsim 0.25$  mag. If these have similar properties to those structures studied in detail, the mass of high- $z$  gas associated with extraplanar dust in NGC 891 likely exceeds  $2 \times 10^8 M_\odot$ , which is  $\sim 2\%$  of the total neutral ISM mass of the galaxy. The absorbing properties of extraplanar dust structures in NGC 891 are best fit with  $R_V \equiv A_V/E(B-V) = 3.6 \pm 0.4$ . A comparison of the new WIYN images with an archival Hubble Space Telescope image of the central region of NGC 891 suggests that the quantities we measure for the extraplanar dust features are not seriously affected by atmospheric blurring in the WIYN images.

Some of the dust features seen in NGC 891 suggest supernova-driven galactic fountain or chimney phenomena are responsible for their production and are clearly associated with ionized gas structures thought to be tracing the violent disk-halo interface of this galaxy. However, other structures are not so readily associated with

---

<sup>1</sup> Based on observations obtained by the WIYN Observatory which is a joint facility of the University of Wisconsin-Madison, Indiana University, Yale University, and the National Optical Astronomy Observatories. Supplemental data are also provided by the NASA/ESA Hubble Space Telescope, obtained from the data archive at the Space Telescope Science Institute. STScI is operated by the Association of Universities for Research in Astronomy, Inc. under the NASA contract NAS 5-26555.

<sup>2</sup>howk@uwast.astro.wisc.edu

<sup>3</sup>savage@uwast.astro.wisc.edu

these energetic processes. We discuss several mechanisms which may produce high- $z$  dust structures such as those seen in the WIYN and HST images presented here. It is, however, less than clear which of these mechanisms are primarily responsible for the extensive extraplanar dust structures seen in our images. The data presented are part of a larger program to search for and characterize off-plane dust structures in edge-on systems.

## 1. Introduction

The processes thought to eject matter away from the thin disks of spiral galaxies will act upon both gas *and* dust. What is the fate of dust grains participating in various types of ejection processes? Are the ejection processes violent enough to completely destroy the grains or is the destruction only partial? Conversely, does the presence of dust in galaxy halos provide important information about the nature of the ejection processes? Are the heavy elements in halo matter mostly found in dust grain cores and thus unavailable for important atomic radiative processes? Does the pressure of radiation acting on interstellar dust help support material in galaxy halos? Do “galactic chimneys” expel clean gas or gas containing dust? Very few of these questions can currently be answered because very little is known about the existence of dust in galaxy halos.

Though interstellar dust grains may play a significant role in the evolution of material undergoing circulation between the disks and halos of spiral galaxies, this role has not received much attention from an observational point of view, and is only beginning to be addressed theoretically. Sofue and his coworkers have suggested that dust filaments they identify in inclined galaxies may be the results of magnetic phenomena or at least may be tracing the magnetic fields in these galaxies (Sofue 1987; Sofue et al. 1994). The Sofue et al. (1994) paper discusses the appearance of the dust features in NGC 253 and suggests various models for the range of dust structure morphologies observed. They argue that the loops and filaments seen in this galaxy are associated with magnetic fields and may be caused by “magnetic inflation” or by radiatively driving dust along magnetic field lines. Unfortunately, the true  $z$ -extents of the dust features identified by Sofue et al. (1994) in NGC 253 are rather uncertain because the galaxy is inclined  $\sim 12^\circ$  from edge-on orientation.

In an interesting series of theoretical papers, Ferrara et al. (1991), Franco et al. (1991) and Ferrara (1993) have recently re-investigated the effects of radiation pressure on dust grains, including the possibility of radiatively driving dust grains to large  $z$ -distances in spiral galaxies. Their work suggests that radiation pressure on grains can have a significant effect on the kinematics of low-halo clouds of material and may be the dominant factor in determining the dust distribution in hot halos of galaxies. Though these workers have begun to address the problem, it is still not clear, theoretically or observationally, what role dust plays in the large-scale circulations that may occur between the disks and low-halos of spiral galaxies.

With this paper we begin a project to study off-plane dust structures in highly-inclined galaxies, the goal of which is to learn more about the interstellar disk-halo interface in galaxies by studying extraplanar interstellar dust. In this first paper we present images of NGC 891 taken with the 3.5-m WIYN telescope under excellent seeing conditions (0.6-0.65'' FWHM). The images show a wealth of dust structures beyond the thin disk of the galaxy, some stretching to  $|z| \gtrsim 1.5$  kpc. Several of these absorbing structures have been mentioned by previous workers, though no in-depth discussion of their properties or discussion of their role in the disk-halo interface exists. While in many ways NGC 891 is not typical of all galaxies, the images presented herein unequivocally state the case for the presence of dust beyond the thin disk of at least one spiral galaxy.

Sect. 2 gives a brief summary of previous observations of extraplanar interstellar material in NGC 891. Sect. 3 describes the observations and our reduction methods; the properties of extraplanar dust in NGC 891 are discussed in Sect. 4, including a discussion of individual features and an analysis of the absorbing properties of the extraplanar dust structures. Sect. 5 compares the WIYN images with archival Hubble Space Telescope (HST) images to assess the degree to which seeing affects our conclusions. Sect. 6 is a discussion of the possible mechanisms for populating the halo of spiral galaxies with dusty material, and Sect. 7 summarizes our principal results.

## 2. Extraplanar Gas in NGC 891

NGC 891 is a well studied Sb galaxy seen near edge-on ( $i \geq 88.6^\circ$ , Rupen 1991). It has been extensively observed over most of the electromagnetic spectrum and has been particularly important for the study of extraplanar gas. The properties of the diffuse extraplanar  $H\alpha$  emission in this galaxy have been discussed by numerous workers (Dettmar 1990; Rand et al. 1990; Keppel et al. 1991; Pildis et al. 1994a). These studies find diffuse ionized gas (DIG) extending to at least 40'' from the midplane of the galaxy, or  $|z|=2$  kpc assuming a distance of 9.5 Mpc (van der Kruit & Searle 1981; Keppel et al. 1991), with some studies finding evidence for DIG extending further than  $|z|=5.5$  kpc (Rand 1997). The recent Rand (1997) study suggests the ionizing spectrum responsible for this gas is significantly harder than that of the local Milky Way thick disk DIG, based upon a comparison of the He I/ $H\alpha$  line ratio in this gas to the upper limit for Milky Way gas derived by Reynolds & Tufte (1995). The inferred gas temperature from his observations is  $T < 10,000-13,000$  K.

Radio continuum studies of NGC 891 have similarly revealed an extended cosmic-ray halo which is generally correlated with the  $H\alpha$  emission (Dahlem, Dettmar & Hummel 1994). The  $H\alpha$  and radio continuum observations suggest a position dependent scale height of  $\sim 0.6 - 1.3$  kpc [Rand (1997) also finds a second component with scale height  $\sim 5-6$  kpc] and show a strong asymmetry, with the NE side of the galaxy having enhanced emission (Dahlem et al. 1994). The radio data show significant polarization, with the orientation of the polarization vectors suggesting

the large-scale magnetic field structure is parallel to the plane through most of the low-halo, though there may be slight deviations toward more vertically oriented fields further from the center of the galaxy (Dumke et al. 1995; Sukumar & Allen 1991). The patterns of polarization in optical and infrared polarization maps have been interpreted as evidence for vertically oriented or non-toroidal magnetic fields through most of the galaxy (Scarrott & Draper 1996; Fendt et al. 1996; Jones 1997; Wood & Jones 1997). The difference in the suggested orientations for the magnetic field may, in part, be due to the differing resolutions of the two data sets, or possibly to optical depth effects in the visible/IR data. Though the ionized halo of NGC 891 is thick enough to provide significant Faraday rotation at longer radio wavelengths, the observations by Dumke et al. (1995) and Sukumar & Allen (1991) at 2.8 and 6 cm, respectively, should be relatively free from the effects of Faraday rotation and provide an accurate measure of the orientation of the magnetic field. Both these studies conclude that the orientation of the field lines is predominantly parallel to the plane of the galaxy.

NGC 891 has been observed in CO by several workers (García-Burillo et al. 1992; Handa et al. 1992; Scoville et al. 1993). García-Burillo et al. (1992) found an extended ( $|z| \lesssim 1.1\text{-}1.5$  kpc) thick disk or “halo” of CO emission within  $\pm 3.5$  kpc of the galaxy center using single-dish observations. They argue that this component cannot be due to a warping or flaring of the disk based upon the velocity structure of the extended- $z$  material. Indeed, Handa et al. (1992) also find evidence for CO away from the midplane in the form of a “molecular spur” that stretches  $\sim 520$  pc into the halo; they do not discuss the existence of an extended thick disk. Scoville et al. (1993) have presented aperture-synthesis data for the CO  $J=1\text{-}0$  transition. They find no evidence for the extended component of García-Burillo et al., though their data are only sensitive to variations on spatial scales  $\lesssim 30''$  ( $\lesssim 1.4$  kpc). The extended component may show evidence for a higher CO ( $J=2\text{-}1$ )/( $J=1\text{-}0$ ) ratio than the disk material (García-Burillo et al. 1992). If this is indeed true, the higher- $z$  material may be warmer than the disk gas; Scoville et al. point out that their observations, made only in the  $J=1\text{-}0$  transition, could possibly have missed an extended warm component.

Both the CO and H I (Rupen 1991; Sancisi & Allen 1979) observations suggest that NGC 891 lacks an appreciable warp. The deviations from the plane in H I are less than 3% of the radius (Sancisi & Allen 1979). Sancisi & Allen, however, argue that the H I disk flares at large distances. They derive a FWHM thickness for the H I layer of  $< 1$  kpc for the inner regions of NGC 891 and  $\sim 1\text{-}2$  kpc for radial distances  $R > 20$  kpc from the center of the galaxy. A flared disk would not explain the extended CO component observed by García-Burillo et al. (see their Sect. 3.2), though Scoville et al. (1993) observe a slight increase in the CO  $z$ -extent with projected distance from the galaxy’s center. Recently, Swaters et al. (1995, 1997) have reported on new, very sensitive H I observations of NGC 891. The new data, and their modelling of these data, suggest that a more appropriate model for the velocity structure and vertical distribution of H I in NGC 891 is a composite model having both a thin and a thick disk, with the latter lagging the former by  $\sim 25$  km s $^{-1}$  (Swaters et al. 1997; see also van der Hulst 1996). These new data also exhibit H I

extending to  $|z| \lesssim 5$  kpc and may show enhanced  $z$ -structure in the regions of the disk that have enhanced  $H\alpha$  and radio continuum emission (van der Hulst 1996).

Bregman & Pildis (1994) and more recently Bregman & Houck (1997) have observed a diffuse X-ray halo surrounding NGC 891 with the ROSAT observatory. This halo has a vertical surface brightness HWHM of  $\sim 2$  kpc; fits to the data suggest a vertical gaussian density scale-height of  $\sim 3.5$  kpc and  $T \sim 3.5 \times 10^6$  K (Bregman & Houck 1997). They calculate the mass of the X-ray emitting gas to be  $\sim 4 \times 10^7 M_\odot$ ; the mid-plane density and pressure best-fit values are  $0.026 \text{ cm}^{-3}$  and  $10^5 \text{ K cm}^{-3}$ , respectively (for filling factors of unity; see Bregman & Houck 1997). Much of the observed emission from the halo of NGC 891 has been interpreted (Bregman & Pildis 1994; Pildis et al. 1994a; Rand et al. 1990; Dettmar 1990) as being at least consistent with the galactic fountain model of disk-halo circulation (Shapiro & Field 1976; Bregman 1980) or the chimney-dominated model of Norman & Ikeuchi (1989). If the hot material traced by the X-ray emission is indeed participating in a fountain flow, Bregman & Houck predict gas is cooling at a rate of  $0.09 M_\odot \text{ yr}^{-1}$ .

### 3. Observations and Reduction

The primary observations presented herein were taken on the night of 3 December 1996 with the WIYN 3.5-m telescope at Kitt Peak National Observatory. The WIYN imager is a thinned  $2048^2$  STIS CCD with  $21 \mu\text{m}$  pixels. Placed at the  $f/6.5$  Nasmyth focus of the telescope each pixel corresponds to  $0.196''$  on the sky, which is  $9.0 \text{ pc}$  at NGC 891 using the adopted distance of  $9.5 \text{ Mpc}$ . The images presented here were taken under non-photometric conditions. This should not affect our analysis, as our measurements rely upon *relative* photometry. The seeing conditions during the observations were excellent ( $0.6''$ - $0.65''$ ).

We obtained B,V and R broad-band images of NGC 891; Table 1 gives the properties of these images. The resolution given in this table refers to the seeing-limited resolution for the WIYN images and is expressed as the FWHM of Gaussian profiles fit to direct measures of stellar image sizes using the IRAF<sup>4</sup> routine *IMEXAM*. The images have been bias-subtracted and flat field-corrected in the usual manner within IRAF. The flat fields were derived from observations of the ‘‘Great White Spot’’ in the telescope dome. Registration of the images was done using a grid of stars common to all of the images, and the rms errors in the alignment of the three images are approximately 5-10% of a pixel. Similarly, we have used several stars, whose coordinates were measured from Digitized Sky Survey images, to solve for the astrometric plate solution coefficients of our images. The rms error in using the plate solution to derive coordinates is approximately  $0.7''$ . The sky background was determined from the average of numerous star-free

---

<sup>4</sup>IRAF is distributed by the National Optical Astronomy Observatories, which is operated by the Association for Research in Astronomy, Inc., under cooperative agreement with the National Science Foundation.

regions throughout the chip.

Part of our work makes use of supplementary observations from WIYN and HST. In Sect. 4.4 we discuss  $H\alpha$  observations taken with the WIYN telescope. These images were taken through a narrow-band interference filter ( $\lambda_{cen} = 6570 \text{ \AA}$ ;  $FWHM = 16 \text{ \AA}$ ), and used R-band images for continuum subtraction. The exposure time and resolution (after slight smoothing) of the final  $H\alpha$  image are given in Table 1. We have also used an archival HST snap-shot image of the central region of NGC 891 to supplement our WIYN images. The details of the reductions and analysis of this image are given in Sect. 5. The exposure time and resolution for this image are also given in Table 1.

## 4. Extraplanar Dust in NGC 891

### 4.1. General Comments

Figure 1 shows a three-color image produced by combining the B,V and R exposures<sup>5</sup>. The CCD was rotated to image the greatest part of the galaxy, hence North lies  $20^\circ$  clockwise from the top of this image with East being similarly offset from the right of the image. The color image has a slightly worse resolution than the original images. We show the B-band view of NGC 891 in Figure 2. North and East are labelled on this image, and the physical scale is given by the bar in the lower left of the figure. One’s eye is immediately drawn to the prevalent filaments of absorbing dust, particularly seen against the light of the stellar bulge. Figure 3(a) shows a close-up of the bulge area from the B-band data, while Figure 4(a) displays a B-band close-up of the region imaged in  $H\alpha$  by Pildis et al. (1994a) to NE of the bulge, approximately 5 kpc projected distance from the center of the galaxy. Figure 5(a) shows the B-band view of the disk to the SW of the central bulge. Figures 3(b), 4(b) and 5(b) show unsharp-masked versions of the same regions, which were produced by dividing the original image by a version smoothed with a gaussian filter having  $FWHM=15$  pixels (135 pc). To alleviate problems of severe over-subtraction, several stars were replaced with the median value of the surrounding pixels in producing the unsharp-masked versions of these images. Regions in the unsharp-masked images where stars have been removed, and hence regions that should be viewed as erroneous, are identifiable by comparing the unsharp-masked versions of the figures with the original B-band data. In these figures the physical scale, measured in the  $z$  and R directions from the center of the galaxy, is given in kpc along the edges; the scale given has the same orientation as that defined by García-Burillo et al. (1992). A number of the more prominent absorbing features are marked in Figures 3(b) and 4(b) for further discussion. Table 2 contains the locations, physical sizes, morphologies and extinction data for each of these complexes; Table 3 contains the quantities derived from these data (see Sect. 4.3). We have chosen these features because they unambiguously reveal dust far from the

---

<sup>5</sup>This image was prepared by Dr. Nigel Sharp of NOAO.

midplane of this galaxy. Practically this implies that we have preferentially chosen relatively thick clouds that lie on the near side of the galaxy. Given the line-of-sight distance ambiguity, we have no assurance that these features are indeed individual connected structures.

On close inspection one can identify features that seem to be rooted in the disk and stretch primarily away from the midplane (e.g., features 4 and 10); other absorbing features seem to be unconnected to the midplane dust lane (e.g., features 5 and 7). It is also interesting to note that the observed features are anything but simple. The appearance of the dust structures is mottled or “chaotic,” in the non-mathematical sense. Much of the complexity may be due to the superposition of several structures along the line of sight, though some features seem quite well aligned (e.g., feature 4), suggesting coherence and physical association. Further, while some of the dusty filaments protruding from the disk are easily associated with regions of star-formation in the disk, others are not. The morphology of some features leads one to think of supernova-driven activity: cones and shell-like structures (e.g., features 10 and 11 below). Others are less suggestive in this respect (e.g., features 1 and 5). There are features tracable to  $|z| \gtrsim 1$  kpc throughout the galaxy. In the central region, where the distribution of background light is more beneficial for probing high- $z$  material, there are clouds that can easily be found 1.5 kpc from the midplane (e.g., features 2 and 7). There is further evidence, which is thus far inconclusive, in color maps of the galaxy for material at least 1.7 kpc from the midplane and possibly beyond. We cannot, at this time, set an upper  $z$ -height to which the dusty material extends.

The lack of a clear asymmetry about the midplane of the galaxy reveals that these structures cannot be attributed to a warp. Given the relatively certain association of some features with star-formation, the evidence for foreground stellar light towards the features (see Sect 4.2) and the new interpretation of the thickened H I distribution (Swaters et al. 1997), we attribute these dust structures to inner galaxy ( $R < 20$  kpc) high- $z$  features rather than structures associated with a flared gas layer at large radii ( $R > 20$  kpc).

We note that Sofue (1987) and Sofue et al. (1994) identify vertical absorbing features emanating from spiral arms in the inclined galaxies NGC 253 and NGC 7331. They argue that these features must stretch vertically, given that they cross several spiral arms and seem to lie mostly-perpendicular to the major axes of the galaxies. The photographs presented in these papers show structures (their “vertical dust streamers,” as well as loops and arcs) reaching heights of  $z \lesssim 1.5$  kpc from their bases, with widths of order 50-100 pc, quantities similar to those derived for the structures listed in Table 2.

The WIYN images of NGC 891 also show what appears to be a background of poorly-defined absorbing structures, particularly against the bulge of the galaxy. This complex background is better seen in the unsharp-masked versions of the B-band image, shown in Figures 3(b), 4(b) and 5(b), which clearly show the wealth of structure that is less obvious than the most prominent features. These less-distinct absorbing features presumably represent a tangled superposition of many individual high- $z$  features at varying distances through the thick disk of the galaxy. Some

of these background absorbing features are distinguishable as filamentary structures in an HST image of the bulge (see Sect. 5 below), though there appears to be a confused web of background absorbers in the higher-resolution HST image as well.

## 4.2. Extinction Properties

The extinction data for the features identified in Figures 3 and 4 are given in Table 2. The quantities  $a_B$ ,  $a_V$  and  $a_R$  are the “apparent extinctions” towards the dust features for the B, V and R bandpasses, respectively (given in magnitudes). We define the apparent extinction  $a_\lambda$  for a given waveband  $\lambda$  as

$$a_\lambda = -2.5 \log(S_{dc,\lambda}/S_{bg,\lambda}) \quad (1)$$

where  $S_{dc,\lambda}$  is the surface brightness measured towards a dust cloud and  $S_{bg,\lambda}$  is the surface brightness of the local background.

We have measured the appropriate surface brightness ratios for individual dust features along five-pixel wide strips that pass through the feature of interest. Thus, each individual strip represents an average of the data over  $0.98''$  or 45 pc. Typically measurements of 10-20 strips, each at a different position, were taken for each dust structure. Where possible the measurements were taken both along strips parallel and perpendicular to the galactic plane, roughly parallel to both the major and minor axes of a dust feature, depending upon its orientation.

Measuring the ratio for an individual strip through a dust structure,  $(S_{dc,\lambda}/S_{bg,\lambda})_i$ , involved defining a background surface brightness, which was complicated by the multitude of absorbers along the line of sight, and measuring an appropriate on-cloud brightness. The background brightness was derived by interpolating between regions in the locale of the feature that seem to be free of dust. For ease of measurement and to minimize contamination caused by seeing effects, the surface brightness towards the dust complex was chosen to be the point giving the minimum value of  $(S_{dc,\lambda}/S_{bg,\lambda})_i$ .

The final ratio  $S_{dc,\lambda}/S_{bg,\lambda}$  used to derive the values of  $a_\lambda$  given in Table 2 was the average of all the individual measurements  $(S_{dc,\lambda}/S_{bg,\lambda})_i$  for a feature. The values of  $a_\lambda$  given in this table are thus spatial averages of the individual features, since each measurement  $(S_{dc,\lambda}/S_{bg,\lambda})_i$  sampled a different position through the structure. While the observations were taken in non-photometric conditions, the measurement of relative surface brightnesses is still valid. We have made no correction for the presence of emission lines in our images. The most significant contaminator is likely H $\alpha$  in the R-band images.

The technique we have adopted to measure the ratio  $S_{dc,\lambda}/S_{bg,\lambda}$  may, in the individual measurements, tend to be systematically influenced by noise features, i.e., the minimum of the ratio is almost always in a negative noise feature, systematically lowering the observed ratio. This is not, in the end, particularly problematic, for the photon noise that systematically affects



the measurements is generally the smallest addition to the mix of uncertainties. Each individual measurement is itself taken from the average of five adjacent  $0.196''$  pixels, and the apparent extinction quoted for a given feature represents the average of many positions along the absorbing dust structure. The photon noise in the individual measurements are certainly less than the uncertainty associated with defining the continuum level, or  $S_{bg,\lambda}$ . Further, the spatial fluctuations of the ratio  $S_{dc,\lambda}/S_{bg,\lambda}$  in the 10-20 measurements taken at different positions along the absorbing feature tends to dominate the photon noise of the individual measurements. The standard deviation of the individual measurements about the mean for a given feature is generally  $\sim 10\%$ . The systematic affect of the photon noise is minor compared to the other uncertainties involved in our measurement scheme.

The values  $a_\lambda$  of Table 2 do not necessarily represent the true extinction,  $A_\lambda$ , which includes contributions from absorption plus scattering, because of scattering into the line of sight. Further,  $a_\lambda$  differs from the true extinction in that there may be stars on the near side of these features whose light is not absorbed by the dust. It is possible, even in light of these problems, to derive approximate properties of the dust in NGC 891. If we define  $x$  as the fraction of galactic light in a given waveband emitted in front of the dust features, we may follow Gallagher & Hunter (1981) and Knapen et al. (1991) by writing

$$S_{dc,\lambda}/S_{bg,\lambda} = x + (1 - x)e^{-\tau_\lambda}. \quad (2)$$

The quantity  $\tau_\lambda$  is assumed to roughly approximate the extinction optical depth through the cloud at wavelength  $\lambda$ , i.e.,  $\tau_\lambda$  contains contributions from pure absorption plus scattering out of the line of sight. With this formulation it is important to note that equation (2) neglects the effects of light scattered off of dust into the line of sight. The scattering phase function for interstellar dust is very forward-throwing. This implies that most of the light scattered from large angles to our sightline will not enter our beam; the fraction that does is likely balanced by scattering of background stellar light out of the beam, implying that  $\tau_\lambda$  is not precisely equivalent to the true absorption plus scattering optical depth. In our application of this equation we will assume that the value of  $x$  is not wavelength dependent. Equation (2) also assumes the absorbing features we identify are localized in space, i.e., not intermixed with the stars, which is likely reasonable given the discrete appearance of the extraplanar dust in our images, though our treatment then also ignores dust that may be smoothly distributed with the stars. The validity of this assumption depends upon the amount of smoothly distributed dust at various distances from the midplane. Kylafis & Bahcall (1987) estimate the isothermal scale height of dust in NGC 891 to be  $z_{dust} \approx 220$  pc, with a visual optical depth through the center of the galaxy  $\tau_o \approx 10.3$ . This implies  $\tau_V(R = 0 \text{ pc}; z = 500 \text{ pc}) \approx 0.4$ ; though by  $z \approx 700$  pc, this value has decreased to  $\tau_V \approx 0.07$ . However, the very structures we are studying in this paper may have played a role in the derivation of the scale height by Kylafis & Bahcall. If the derived scale height is not appropriate for the smoothly distributed dust, but is significantly increased by the presence of the discrete features, any correction we might make to our analysis would be overly large. The majority of the features we discuss in detail are at heights where the adverse effects of ignoring

a smoothly distributed component are likely relatively minor. At this point, we will neglect the addition of a smoothly distributed dust component in our analysis.

We will assume that the dust in NGC 891 has extinction that is compatible with the parameterization of Cardelli et al. (1989, hereafter CCM), which describes Galactic interstellar extinction with the single parameter  $R_V[\equiv A_V/E(B - V)]$ . The Galactic average for the diffuse interstellar medium is  $R_V \approx 3.1$ , though this value seems to vary with environment (CCM, Savage & Mathis 1979). Using equation (2) and the apparent extinction data in Table 2 it is possible to constrain the value of  $R_V$  for the features seen in NGC 891. Figure 6 shows a plot of  $a_B$  and  $a_R$  versus  $a_V$  for a sample of 36 dust features, not all of which will be individually discussed here. Also plotted are the predicted values of these quantities for various values of  $x$ , using the CCM parameterization with  $R_V=3.6$ , the value of which defines the slope of the relationships between the various wavebands. One can see that the data points for  $a_B$  and  $a_R$  for  $a_V \lesssim 0.7$  describe well the trends expected for CCM Galactic extinction. Furthermore, this is in a regime where effects of the uncertain value of  $x$  are relatively small. Therefore it is possible to constrain the value of  $R_V$  with the low-apparent extinction data for NGC 891. We have minimized the combined  $\chi^2$  of  $a_B$  and  $a_R$  vs.  $a_V$  about CCM models of differing  $R_V$ . Using the variance of the individual measurements of  $a_\lambda$  about the mean given for the features in Table 2, we estimate the errors in the apparent extinctions to be  $\pm 10\%$  ( $\sigma_{a_\lambda} \approx 0.1$  mag.). The minimization of  $\chi^2$  using the estimated errors in  $a_\lambda$  yields  $R_V = 3.6 \pm 0.4$  as the best fit to the data. This value is roughly consistent with the average  $R_V$  for Milky Way disk clouds. For illustrative purposes, we have also plotted dashed lines for  $R_V=3.2$  and  $4.0$ ,  $x=0$  on Figure 6, which represent  $1 \sigma$  deviations from the best fit value of  $R_V$ .

### 4.3. Derived Properties of Individual Dust Features

Equation (2) may be used to derive information on the individual features identified in Figures 3 and 4. Let us assume a CCM extinction law with  $R_V \approx 3.6$ , which implies  $\tau_B = 1.29\tau_V = 1.68\tau_R$ . This allows us to solve for the best values of  $x$  and  $\tau_V$ , using equation (2) in B, V and R. Table 3 gives the derived values of the V-band extinction  $A_V[= 1.086\tau_V]$  and  $x$  for the individual features discussed in Sect. 4.4 and identified in Figures 3 and 4. In general the values of  $A_V$  and  $x$  change by  $\pm 10\text{-}15\%$  as one changes the assumed value of  $R_V$  by  $\pm 1\sigma$ . The greatest contributor to the uncertainties in these values is likely our neglect of scattering, however.

Bohlin et al. (1978) used the *Copernicus* observatory to show  $N(\text{H I}) + 2N(\text{H}_2) \equiv N_H \approx 5.8 \times 10^{21} E(B - V)$  [ $\text{cm}^{-2}$ ] in the disk of the Milky Way. Here  $N(\text{H I})$  and  $N(\text{H}_2)$  are the H I and H<sub>2</sub> column densities, respectively, and  $N_H$  is the total hydrogen column density, not including the contribution from ionized gas. To estimate the amount of gas associated with the absorbing dust structures, we apply this relationship between gas and dust to the extraplanar features in NGC

891. Assuming  $R_V \approx 3.6$ , we use

$$N_H = 1.7 \times 10^{21} A_V [\text{cm}^{-2}] \quad (3)$$

to estimate the column density of associated gas in the observed dust structures. This estimate, when coupled with the approximate projected area of a given structure, yields a mass estimate of each feature; both quantities are given in Table 3 for the features discussed herein. The mass estimate given here includes a correction factor of 1.37 to convert from the mass of hydrogen to the total mass accounting for typical fractions of helium and the heavy elements. The values of  $N_H$  derived using equation 3 are only appropriate if the gas-to-dust ratio in the observed structures is approximately that of Milky Way disk clouds; this will be an underestimate of the column density if significant dust destruction has occurred, an overestimate if the dust has been separated from the gas (see Sect. 6). Our estimates for the column density of material vary by  $\pm 15\text{-}20\%$  as the value of  $R_V$  is changed by  $\pm 1\sigma$ .

Except in cases of significant  $\text{H}\alpha$  contamination in the R-band images, the measurements we have made will tend to underestimate the apparent extinctions due to difficulties with the definition of the background surface brightness,  $S_{bg,\lambda}$ , and thus underestimate the optical depth and column density. The quantities given in Table 3 for features whose extinction measurements may be contaminated by  $\text{H}\alpha$  emission are marked with a colon, indicating a greater degree of uncertainty in the derived values of  $A_V$ ,  $N_H$  and mass. We further underestimate the optical depth due to the effects of light scattered into the line of sight by the dust. Our estimates of the quantities given in Table 3 are therefore to be considered lower limits.

In general our estimates of the gas column densities associated with the observed dust absorption give  $N_H \gtrsim 10^{21} \text{ cm}^{-2}$ . These estimates place the individual features in the high end of the realm occupied by diffuse clouds in the disk of the Milky Way. If we assume the depths of the features are similar to their widths, we obtain density estimates of  $\langle n \rangle \sim 3 - 20 \text{ cm}^{-3}$ . Many of the features are likely to include molecular material if these estimates of column and particle densities are correct. For Milky Way disk gas, the average value of the molecular fraction [ $f \equiv 2N(\text{H}_2)/N_H$ ] for material towards stars having  $0.3 < E(B - V) < 0.53$ , or  $0.9 \lesssim A_V \lesssim 1.6$ , appropriate for most of the structures in Table 3, is  $\langle f \rangle \approx 0.22$  (Savage et al. 1977). Thus nearly one-quarter of the hydrogen content of the extraplanar features may be tied up in molecules, if the gas content and physical conditions of the dust structures are similar to those in the disk of the Milky Way, a possibly dubious assumption. The predicted masses for these features are quite large: the masses given in Table 3 are similar to those for the Galactic giant molecular clouds. The sizes of most of the structures discussed here, however, are significantly larger than those for typical GMCs (sizes  $< 100 \text{ pc}$ ).

If the hydrogen in these structures is mostly atomic, the values of  $N_H$  given in Table 3 are above the detection limits of the H I surveys of Rupen (1991) and Sancisi & Allen (1979); however, the individual features discussed here would be unresolved and almost impossible to identify. Indeed, some of the features apparent in our WIYN observations are washed out in

images with seeing worse than  $1.0''$ . The CO observations of Scoville et al. (1993) and Handa et al. (1992) begin to be able to resolve some of the structures. A comparison of our images with the total intensity map of Scoville et al. shows some correspondences near the bases of several dust structures (e.g., feature 1), though the CO data do not show material much above  $|z| \sim 500$  pc. The correspondences may simply be coincidence. Unfortunately, the molecular spur discussed by Handa et al. (1992) lies near the bright star seen just above the plane in Figure 2(b); we are not able to measure reliable surface brightnesses for that feature given the slope of the background light and the contamination from the bright foreground star. García-Burillo et al. (1992) obtained several observations towards directions that showed dust features extending beyond the thin disk of NGC 891; they find no clear difference in the CO properties of sightlines on or off of these dust structures, though they sample few of the prominent dust features. Their spectra towards dust features have broad velocity widths and suggest a CO component extended along the line of sight, which they argue may be evidence for CO emission independent of the vertical dust features. The tangle of structures seen between the prominent features discussed here is evidence for dust filaments far along the line of sight into the low-halo of the galaxy. The CO observations may therefore be detecting many structures along the path through the thick disk.

Given the derived extinctions and column densities given here, which imply quite thick dust structures, we might expect to be able to observe thermal emission from the dust itself. Guélin et al. (1993) have mapped NGC 891 at 1.3 mm using the IRAM 30-m telescope. Their data show cold dust along the major axis of the galaxy, but they do not mention the vertical extent of the material, nor does there appear to be significant thermal emission in their map associated with the most obvious dust features seen in our images. NGC 891 was observed with IRAS using the Chopped Photometric Channel. The emission from NGC 891 at 50 and 100  $\mu\text{m}$  was unresolved perpendicular to the plane with this instrument, which at these wavelengths has a resolution of  $\sim 75''$  and  $85''$  respectively (Wainscoat et al. 1987). In general observations that may have shown thermal emission from extraplanar dust have been hampered by insufficient resolution or sensitivity to measure dust beyond the thin disk of the galaxy.

Using the masses given in Table 3, we may make estimates for the gravitational potential energies of the observed structures given their positions above the midplane. Approximating the distribution of mass density using the isothermal sheet model ( $\rho \propto \text{sech}^2(z)$ ; though see van der Kruit 1988), the potential energy  $\Omega$  of a structure at a height from the midplane  $z$  is

$$\Omega = 10^{52} \text{ergs} \left( \frac{M_{cloud}}{10^5 M_{\odot}} \right) \left( \frac{z_o}{700 \text{pc}} \right)^2 \left( \frac{\rho_o}{0.185 M_{\odot} \text{pc}^{-3}} \right) \ln[\cosh(z/z_o)] \quad (4)$$

where  $M_{cloud}$  is the mass of the dust cloud,  $z_o$  is the mass scale height of the (stellar) disk and  $\rho_o$  is the mass density at the midplane. The value  $z_o = 700$  pc used here is from a fit to the stellar light in near-infrared images of NGC 891 (Aoki et al. 1991), which we will assume approximates the mass density scale height, and we have adopted the mass density  $\rho_o = 0.185 M_{\odot} \text{pc}^{-3}$  appropriate for the solar neighborhood (Bahcall 1984). The relationship given in equation 4 is likely not appropriate for material very near the midplane or beyond  $z \approx 1.5$  kpc, with the

high end being more uncertain (Aoki et al. 1991; Kuijken & Gilmore 1989). Though this series of approximations may not lead to highly accurate potential energies, it is interesting to examine these order of magnitude estimates. It should be noted that this equation gives only the potential of the material at a given height  $z$ . It makes no assumptions as to the fraction of input energy that is radiated or converted to purely thermal motion, which would certainly be important in most expulsion scenarios (see discussion in Sect. 6). Thus if used to approximate the input energy required to lift the material from  $z = 0$  to its observed height, the energies derived must be treated as lower limits. Further, no kinematic information for these structures exists, so no estimate of the kinetic energies of these dusty structures can be made, again making the energies calculated with equation 4 lower limits to the total input energy. Indeed, these structures may be at mid-points in their evolution, and the processes responsible for forming these structures may still be depositing energy into them, adding even more energy to the mix. In Table 3 we give the approximate energies derived using equation 4. For structures extended in  $z$  we have used a central value for the  $z$ -height of the feature in deriving the energy. The energies given in Table 3 are quite large, but similar to those derived for supershells in the Milky Way (Heiles 1979). Those values given in Table 3 are equivalent to the kinetic energy input into the ISM of tens to hundreds of Type II supernovae, though the input energy required to lift the observed features from the midplane is greater than this due to radiative and thermal losses.

#### 4.4. Notes on Individual Features

We have derived the properties for a set of individual dust features seen far from the plane of NGC 891. We have not attempted an unbiased selection of the individual structures, but rather have chosen some of the more “interesting” and clearly visible features. In general we have selected relatively small structures that are more likely to represent coherent structures and are relatively easily seen in hardcopies of the images.

Our analysis of these individual dust features gives striking numbers. The features are characterized by  $N_H \gtrsim 10^{21} \text{ cm}^{-2}$ , with masses estimated to be more than  $2 \times 10^5 - 5 \times 10^6 M_\odot$ , assuming Galactic gas-to-dust relationships. These numbers are quite large, and may imply the presence of a significant amount of molecular material, as mentioned earlier. The gravitational potential energies of the individual dust structures are similarly large:  $20 - 240 \times 10^{51} \text{ ergs}$ , which represents the energy input of at least tens to hundreds of supernovae, possibly an order of magnitude more.

The absorbing structures observable far from the plane of NGC 891 have a wide range of morphologies, and even of physical properties. One of the more extreme examples of these individual features is feature 1, which lies to the SW of the galaxy’s center. The derived mass estimate places it at the high end of the mass range for the Galactic giant molecular clouds. It is quite opaque and may harbor a significant amount of molecular mass. There is some evidence for a slight  $z$ -extension of CO gas at the base of this feature in the maps of Scoville et al. (1993).

Very deep interferometric CO observations of this galaxy might yield emission from high- $z$  dust features such as this one.

Feature 7 is quite interesting for its morphology; it appears as a cometary-shaped absorbing feature 1.4 kpc from the mid-plane. There is also lightly-absorbing material seen “trailing” this feature at higher  $z$ . There are several other features at similar  $z$ -heights that seem to have similar morphologies; unfortunately, the apparent extinctions in the V and R bands for many of these are too low to measure in the current data set. Deeper observations will allow us to probe dust higher into the halo of NGC 891.

Among the most interesting of the individual structures, particularly in the context of the disk-halo interface in galaxies, are features 10 and 11. These structures lie in the NE portion of the disk of NGC 891 and are almost certainly connected with the star-formation activity on this side of the galaxy. This region shows enhanced  $H\alpha$  emission, as well as several structures whose shapes are reminiscent of supershells (Rand et al. 1990; Pildis et al. 1994a). Given the known presence of  $H\alpha$  emission near these two features, though seemingly slightly offset, the quantities derived for these two structures should be considered more uncertain than those derived for the previously discussed features due to  $H\alpha$  contamination in the R-band image.

Feature 11, which appears as an arc open to high  $z$ , outlines an  $H\alpha$  emitting ionized shell quite well. The “walls” of the dusty shell are approximately 50-60 pc thick with a maximum separation of almost 600 pc. The center of the shell is itself  $\sim 600$ -650 pc above the midplane. The two sides of this structure have different absorbing properties. In Table 2 we refer to the southern-most side, which is closest to the bulge of the galaxy, as 11a and the northern-most as 11b.

Feature 10 appears as a cone of dusty material, reaching to a maximum traceable height of  $z \approx 900$  pc. The apparent opening angle of this feature is  $14^\circ$ . Ionized gas appears brighter along the exterior of the cone-like structure, tracing its outer boundary very well.

To show the relationship between the ionized gas structures and the absorbing dust features, we compare the B-band image and an  $H\alpha$ + $[N\ II]$  image of the NE section of NGC 891 in Figures 7(a) and (b). These relatively shallow  $0.9''$  resolution images were taken at WIYN through a filter not optimized for the redshift of NGC 891 ( $\lambda_{cen} = 6570 \text{ \AA}$ , FWHM =  $16 \text{ \AA}$ ). The response to  $H\alpha$  changes as a function of position along the disk, given the rotation of the galaxy, and the relative throughput of  $H\alpha$  vs.  $[N\ II]$  also varies along the disk. Even given the non-optimal filter characteristics, the image is useful for comparison with the dust structures seen in this portion of the disk. One can see structures in ionized gas associated with the dust features 10 and 11, particularly the almost circular bubble-like feature that is outlined by the dust of feature 11. The edges of the cone-like feature 10 are also bright in ionized gas emission. This region of the galaxy shows very pervasive ionized gas. The star-formation rate is thought to be very high in this section of the disk, and our data reveal a plethora of ionized regions that are powered by young stars in the disk. The color image shown in Figure 1 shows that these regions appear quite blue, also

indicating the presence of massive stars.

The H $\alpha$ + [N II] images reveal that some of the dust structures observed in NGC 891 do have counterparts tracable in ionized gas, while others show no detected ionized gas emission. There is a quite robust association of features 10 and 11 with energetic processes driven by the existence of hot stars. An in-depth comparison of the relationships of these and other structures with counterparts seen in ionized gas will require deeper H $\alpha$  images through a more appropriate filter and will be the subject of future work.

#### 4.5. The Dusty Thick Disk

While we have concentrated our discussion thus far on some of the more prominent features, a large ensemble of less distinct or smaller high- $z$  extinction structures are apparent in the WIYN images. Number counts of these features are difficult to make because we have no objective criteria for what constitutes an individual structure; chance superposition of several clouds along the line of sight through the galaxy are almost certainly producing some of the structures we might by eye identify as singular features. We are also unlikely to pick up low column density material or features that lie very far into the galaxy; indeed, we would be unable to identify even large optical depth features with  $x \gtrsim 0.6 - 0.7$ . We have, however, attempted a rough number count of high- $z$  dust features in the halo of NGC 891. We make no claims as to the completeness of such a count. We have been relatively conservative in identifying structures, and therefore our counts represent a lower limit to the number of features. Our rough number count for structures having  $|z| \gtrsim 400$  pc and  $a_B \gtrsim 0.25 - 0.3$  mag. yields more than than 120 features. If these features exist on the front side of the galaxy, with no intervening stars, then  $a_B \sim A_B$  and  $N_H \gtrsim 4 \times 10^{20} \text{ cm}^{-2}$  for these features, neglecting scattering.

Counts taken along lines at  $z = \pm 500$  yield approximately 30 features ( $a_B \gtrsim 0.3$ ) on each side of the galaxy within the central  $\pm 3$  kpc projected distance from the center of the galaxy; similar results are obtained for counts at  $z = \pm 700$  pc. There is no evidence for an asymmetry in the number of counts across the midplane of the galaxy, as one might expect if a warp were the cause of these dust features. Unfortunately, comparisons between the number of features per kpc in either the radial or vertical directions are severely hampered by the exponential decay of the background illumination.

The 12 structures identified in Figures 3 and 4 together contain  $\sim 2 \times 10^7 M_\odot$  of material, if the assumption of Galactic gas-to-dust extinction ratios is appropriate. If the 120 features we count have properties similar to those discussed above, then the mass tied up in the visible structures with  $|z| \gtrsim 400$  pc may be  $> 2 \times 10^8 M_\odot$ . This represents  $> 2\%$  of the total mass of neutral gas, H I+H $_2$ , in NGC 891, estimated to be  $\sim 9 \times 10^9 M_\odot$  (García-Burillo et al. 1992).

It is clear that there are a large number of absorbing structures far from the mid-plane of NGC 891 that may contain a significant amount of mass. We associate this material with the

known thick disks of neutral and ionized hydrogen in NGC 891 (Swaters et al. 1997; Dahlem et al. 1994; Dettmar 1990; Rand et al. 1990). This association is only based upon the fact that the dust far from the plane shows a similar extent to the gaseous components of the thick interstellar disk of NGC 891. Our images show that the dust associated with the thick disk is quite structured, not smoothly distributed. Indeed, the  $H\alpha$  thick disk is broken up into filamentary structures (Dettmar 1990; Rand et al. 1990). However, deep high angular resolution observations of  $H\alpha$  emission do not exist. Therefore, a detailed comparison between the extraplanar dust structures and  $H\alpha$  structures will require new observations.

In future work on this galaxy, we will attempt to better our quantitative understanding of the distribution of dust, particularly searching for evidence of a two-component distribution of the dust. The existence and properties of a dusty thick disk are important for understanding the processes that eject material far from the plane and the relationship of the dust to other tracers of the interstellar thick disk, as well as for correcting for the effects of dust upon other observations (e.g., derivation of  $H\alpha$  scale-heights). However, the derivation of the thick disk dust scale height is rife with difficulties, and hence we have not attempted it in this first paper on the extraplanar dust of NGC 891. The derivation of such a scale height is heavily dependent upon a correct model for the distribution of stellar light in the galaxy, particularly for the presence of a stellar thick disk (see Morrison et al. 1997). Correct fitting the observed light distribution to determine the distribution of dust also requires a good treatment of the radiation transfer through the galaxy. Kylafis & Bahcall (1987) have studied the distribution of stars and dust in NGC 891, though they assume a one-component model for the dust. Whether adding a thick dusty disk better fits the photometric data remains to be seen.

## 5. HST Images and Seeing Effects

NGC 891 was observed by HST in the imaging snap-shot survey of Illingworth et al. (HST Prop. 5446). We have retrieved the Wide Field/Planetary Camera 2 (WFPC2) images from the HST archive; the images cover the central region of the galaxy and are useful for comparing with our WIYN images. Table 1 gives the properties of the HST WFPC2 images. The two 90-s exposures taken with the F606W filter were co-added and mosaiced within IRAF; the final WFPC2 image is presented in Figure 8. The resolution of the image is  $0.1''$ , and is therefore a good measure of the degree of degradation caused by seeing effects in the WIYN images.

We have measured the widths (short axis) of all of the features identified in Table 2 that are contained within the WFPC2 image (features 1, 2, 3 & 4) as well as several other features common to the images. We use the WIYN V-band image for these measurements, which is a good match to the F606W filter used in the HST observations (see below). The measurements of features in the HST images agree with those measured in the WIYN images to about one or two WFPC2 pixels, or 5-10 pc. This correspondence is excellent considering the general complexity of the absorbing features.



While the HST image shows the features on a finer scale, the bulk of the apparent structure in the most prominent absorbing regions is resolved by WIYN. Some of the features show more filamentary edges and overall structure in the HST image. There are a few instances of features that are washed out by the seeing at WIYN but are detected in the HST image. However, there are also low-contrast features at high  $z$  that are detected in the WIYN images but not the HST image. The HST image more clearly resolves into individual features some of the absorbing material that lies further along the line of sight into the galaxy. As discussed above, there still exists a tangle of overlapping features that can be picked out, but not distinguished, in the HST image.

To more clearly show the difference between the WIYN and HST views of NGC 891, we present close-up views of the WIYN B-band and HST images for features 1 and 2 in Figure 9 and for features 3 and 4 in Figure 10. The HST images do show that there are structures on finer scales than can be detected with WIYN; however, the bulk of the structure seems to be apparent in the WIYN images. Though the HST image provides a factor of six better resolution, the larger features identified in the WIYN images do not break down into separate structures in the HST image. While they may still be superpositions of several clouds along the line of sight, few if any of the structures that seem to be connected in the WIYN images are separable into distinct structures at the resolution of the HST image. Feature 4 is an example of this (see Figure 10). In the WIYN image, it gives the appearance of being a mostly-coherent structure stretching over several hundred pc. The HST image reveals nothing that contradicts this immediate impression.

The WFPC2 F606W filter is centered at  $\lambda = 5957 \text{ \AA}$ , approximately midway between the centers of the V and R filters used with WIYN, but is very broad, having approximately the same short-wavelength cutoff of the V filter. A convolution of the F606W filter transmission curve with the expected flux distribution produced by  $T_{eff} = 5,000$  and  $10,000$  K stars subjected to CCM extinction curves yields  $\langle A_{F606W}/A_V \rangle \approx 0.97$ , independent of  $R_V$  (using Kurucz 1991 atmospheres; see Cole et al. 1991). This is not particularly surprising since, although the F606W filter extends much further into the red than does the V-band filter, the extinction over this bandpass is dominated by the short-wavelength end (at least for a flat-spectrum source). We have measured the apparent extinctions of many of the features common to both the WIYN V-band and HST F606W images as prescribed in the last subsection, though we have used 10 pixel wide cuts for the HST image to account for the difference in pixel size.

As discussed above, the result is a spatial average of the apparent extinction for a given feature. Using the standard deviation of the individual cuts about the mean for a feature as an estimate of the error, our measurements of absorbing properties for structures in both images typically agree within one standard deviation. There are, however, a few features for which this is not the case. These are typically characterized by having a “core/halo” structure, i.e., a central very opaque feature surrounded by a less-absorbing region. The discrepancy in apparent extinction arises because we adopt the minimum brightness ratio,  $S_{dc,\lambda}/S_{bg,\lambda}$ , as representative of the whole. When deriving the brightnesses from the WIYN images, our individual measurements

have a similar resolution in both dimensions, using cuts with widths of 5 pixels combined with a seeing-limited resolution of 3-4 pixels in the perpendicular dimension. The HST measurements are less likely to be an average in both directions, having cuts of  $0.1'' \times 1.0''$  through each feature. Measurements of features in the HST image, given our technique, sample the most opaque regions of these “core/halo” structures and are less an average of the cloud as a whole. Though our measurements of apparent extinctions for various features show some discrepancies, we believe the method generally gives information appropriate for deriving the spatially-averaged properties of the absorbing structures.

## 6. Discussion

From the images presented herein it is immediately clear that clouds of dust, if not dust and gas, exist at large distances from the midplane of the spiral galaxy NGC 891. It is not known how common these extraplanar dust clouds are in spiral galaxies, nor is it clear that the absorbing structures seen in this galaxy are all caused by the same phenomenon; even given these uncertainties, it is important to begin a discussion of mechanisms that may be responsible for the features we see in the WIYN and HST images of NGC 891. Although small quantities of dust at large distances from the planes of galaxies can be produced by direct injection from evolved stars and supernovae, it appears for galaxies like NGC 891, with extensive dust structures at large  $z$ , that some type of ejection process from the reservoir of material in the disk is required to produce the amount of high- $z$  material seen. Further, the complex morphologies of the structures seen in our data strongly suggest mechanisms other than direct injection for producing these absorbing features. In the following we discuss four types of ejection processes: 1. Hydrodynamical phenomena, including fountain flows. 2. Expulsion by radiation pressure on dust. 3. The effects of magnetic fields, and 4. ejection mechanisms involving dynamical instabilities.

### 6.1. Ejection via Hydrodynamical Phenomena

It may be possible to transport dust from the thin disks of spiral galaxies via hydrodynamical phenomena such as “galactic fountain” flows (Shapiro & Field 1976; Bregman 1980; Houck & Bregman 1990) or “galactic bores” (Martos et al. 1996, cf. Suchkov & Shchekinov 1975). The expulsion of dust in these scenarios would seem to depend sensitively upon the physical conditions at the sights of expulsion, e.g., supershells for the fountain model. In the fountain model there are two possibilities for lifting dust beyond the thin disks of spirals. The first relies upon the upwelling hot gas to carry the dust. This mechanism seems unlikely to be able to transport a large amount of dust, either by entrainment of material as the hot gas escapes the disk or by feeding the dust into the hot interiors of supershells prior to the expulsion of the hot material, due to the extremely low density of the hot gas and the harsh conditions within this hot medium. Ferrara et al. (1991), in their numerical models of dust behavior when immersed in a hot coronal halo, find that the

dust is able to move relatively unimpeded in such conditions. The inverse is likely also true: when the hot gas is expanding out of the disk of the galaxy, it may not offer much lift to the dust.

Possibly more likely is the transport of dusty material from the thin disk within the dense walls of supershells. While the initial expansion of a supernova remnant or superbubble (SNR) may cause strong shocks, through most of their evolution SNRs expand at relatively low velocities. In this slowly moving phase a remnant sweeps up considerable mass which does not experience shocks with large velocity jumps. Thus the dust swept up in this phase of SNR evolution may remain relatively intact, i.e., the shocks dust may encounter in this phase are not sufficiently strong to destroy large fractions of the grains. As a superbubble expands into the halo, it transports this undestroyed dust upwards within its walls. The chimney model of Norman & Ikeuchi (1989) suggests that if the supershells are able to break out they will leave remnant, kiloparsec-scale vertically-oriented walls, which may be dust-laden. Indeed, Koo et al. (1992) have identified many candidate Galactic “worms” in both H I and IRAS 100  $\mu\text{m}$  emission that may be such remnants or the walls of supershells themselves. The absorbing features seen in our images may be pronounced examples of these dusty worms, particularly the features found in the NE section of the disk. Feature 11, for example, seems to be the dusty wall of a known H $\alpha$  supershell.

Dense knots of material which follow ballistic trajectories may also be expelled from the disk by superbubbles. Knots formed by Rayleigh-Taylor instabilities as a superbubble breaks through the disk material and begins to accelerate into the halo follow ballistic trajectories away from the disk, as they have significantly higher column densities than the halo material (Cioffi 1986). These knots of material may lead to relatively disconnected clouds of dense material in the low-halo of spiral galaxies. If dust survives in these fragments of the evolved superbubble, the ejected clouds may provide a source of halo dust grains. Greater knowledge of the degree to which dust can survive in the walls of supershells is needed to assess the role these structures may play in lifting dust beyond the thin disk of spirals.

Models which predict upwelling gas trajectories as material “falls” into the enhanced gravitational potential of a spiral arm, such as the “galactic bore” model of Martos et al. (1996), may also exhibit a sensitive dependence upon the prevailing local conditions. The depth of the gravitational potential well into which the material falls and the velocity with which gas encounters the spiral density wave would both be a determining factor in the resulting temperature of the gas (Kovalenko & Levy 1992). Thus the prevailing physical conditions where the upwelling gas is expected to be produced would depend upon the location of the gas with respect to the corotation radius, since the velocity with which gas enters the density wave depends upon its location relative to corotation, and the amplitude of the density wave. Dust grains in material that encounters too strong a shock as it falls into the enhanced gravitational potential of a spiral arm may be too efficiently destroyed to produce substantial high- $z$  opacity, even if the gas-dust drag were sufficient to lift the grains as the heated gas expands upwards into the low halo.

The literature on the effects of either model (fountain vs. bore) on dust grains and their

distribution is quite sparse. Much work needs to be done, both observationally and theoretically, before a reasonable discrimination can be made between these types of models and those that rely on other processes to lift grains from galactic thin disks.

## 6.2. Ejection via Radiation Pressure

Ferrara et al. (1991), Franco et al. (1991) and Ferrara (1993) have suggested that radiation pressure on dust grains can play a significant role in the kinematics of both the gas and dust in spiral galaxies. Franco et al. (1991) investigated the effects of radiation pressure on dusty clouds in the thick interstellar disk of the Milky Way, and by extension other spirals. Their results suggest that interstellar clouds having gas-to-dust ratios typical for Milky Way clouds can be “photolevitated” to a few hundred parsecs above the midplane of the Galaxy. Clouds directly above luminous star clusters or near spiral arms may be lifted to even greater heights. Ferrara (1993), extending this work, suggested the vertical support of the neutral interstellar thick disk of the Milky Way (Lockman 1984) could be provided by turbulence when including the stellar radiation field, which lowers effective gravitational potential of the dusty material.

In contrast to the studies above, which discuss the distribution of clouds near the midplane, the calculations of Ferrara et al. (1991) follow the trajectories of dust grains immersed in a hot hydrostatic galactic corona. They find that dust can be expelled from a model Milky Way disk to quite large distances ( $z \sim 20 - 120$  kpc). It should be noted, however, that they include no diffuse clouds beyond the  $z = 200$  pc initial position of the grains. Diffuse clouds above the plane, even if they fill a small fraction of the grains’ trajectories through the halo, could cause significantly more drag than the models of Ferrara et al. Warm neutral clouds are known to exist at large  $z$ -heights in our Galaxy. The thick disk of neutral material or “Lockman layer” discussed above extends to  $z$ -heights in excess of 500 pc (Dickey & Lockman 1990), while intermediate velocity clouds may lie significantly higher (e.g., Wakker et al. 1996). However, the influence of magnetic fields may be the most significant modifier to the dust trajectories of the Ferrara et al. models (see below).

More recently Ferrara & Shull (as discussed in Ferrara 1997) have begun modelling the time evolution of the dust distribution in the immediate vicinity of OB associations via Monte Carlo models. Their models account for the more extended  $z$ -component of H I and for the evolution of the radiation field of the OB association. They find that dust can be expelled well beyond the thin interstellar disk of their model galaxy and predict a relatively flat distribution of dust grains above these collections of stars. The models further predict that small grains tend to be expelled to greater distances than large grains. In the early evolution of their “dusty chimneys,” the distribution of dust in their simulations is roughly conical, with the base of the cone pointing away from the midplane; this morphology is not unlike that of feature 10. This work seems quite promising, for it includes the influence of the interstellar thick disk and makes predictions that should be testable with high spatial resolution infrared images of edge-on galaxies (e.g., with SIRTf or SOFIA, which could be used to search for evidence for a varying degree of dust

destruction or changing gas-to-dust ratios with  $z$ ).

A concern with models that rely upon radiation pressure to expel material from the disk of a galaxy is the relatively large optical depths we have derived for the high- $z$  features identified in Figures 3 and 4. Dust clouds that are self-shielding would seem to be difficult to drive radiatively and may be subject to radiation-induced instabilities. Indeed, Franco et al. (1991) argue that clouds having  $N_H \gtrsim 5 \times 10^{20} \text{ cm}^{-2}$  or  $A_V \gtrsim 0.3$ , assuming Milky Way gas-to-dust ratios, are unable to be driven effectively. This is at least a factor of two below our lowest column density/extinction estimates given in Table 3. Those features that stretch as “columns” vertically away from the plane may have even larger column densities and optical depths when viewed from the disk of NGC 891 (e.g., features 1 and 4).

In general radiative expulsion models predict lesser amounts of grain destruction than those methods that rely upon violent means, such as the fountain-type models, though little work has been done theoretically to describe the extent to which dust is transported or destroyed in supershells. Ferrara et al. (1991) have calculated that bare silicate grains lose some 20% of their mass in their  $\sim 2 \times 10^8$  yr trip through a model galactic corona, with graphite grains losing even less; this time scale is similar to that of total destruction for grains in the disk of a galaxy which are exposed to the passage of multiple supernova shocks (Jones et al. 1994). Jones et al. (1994) calculate the fraction of grains destroyed in the passage through a strong shock is  $\leq 0.29$  and  $\leq 0.45$  for graphite and silicate grains, respectively. If grains pass through a strong shock and find themselves in the harsh hot interior of a supershell, the fraction of grain destruction may be greater than this value.

A further difference between the Ferrara et al. (1991) predictions for the destruction of grains in a hot halo, and for the destruction one might envision in a fountain-like scenario, is that the destruction of grains in the radiatively driven scenario primarily occurs far from the disk of the galaxy. In a supernova-driven expulsion scenario, the bulk of the dust destruction should occur within the first kpc. A clear examination of the distribution of elemental depletions with distance above the plane of our own Galaxy may help to distinguish between these two types of models. Abundance studies with HST (Sembach & Savage 1996) reveal that grain cores survive the processes that lift matter to  $z$  distances ranging from 0.5 to 1.5 kpc in the halo of the Milky Way. Indeed, our WIYN images of NGC 891 provide the same information for an external galaxy: grains survive the trip from the galactic plane to the low-halo, by whatever means they are expelled. These observations imply that the cores of dust grains are very resilient and survive while being pushed into the halo by violent processes, or reach high- $z$  by less extreme means, such as via radiation pressure.

Knowledge of the dust properties of supershells in the Milky Way and in other galaxies may constrain the amount of dust that is destroyed in these structures and help determine whether they are able to expel dust from the thin disks of spirals. It may be possible to search for evidence of grain destruction in the dust features we have discussed here using emission line imaging or

spectroscopy of the near-infrared [Fe II] and Pa $\beta$  lines. The [Fe II]/Pa $\beta$  ratio is known to be enhanced in regions of supernova activity as the dust is destroyed, freeing Fe from the solid phase (Greenhouse et al. 1991). The presence of enhanced [Fe II] emission (over typical H II regions, say) would be an indicator of dust destruction and likely supernova activity. High-resolution images would be required to search for emission from specific features; HST, with the newly installed NICMOS instrument, might be useful for doing exactly this.

### 6.3. The Effects of Magnetic Fields

Recent radio continuum observations at 2.8 cm (Dumke et al. 1995; see also Sukumar & Allen 1991), where the effects of Faraday depolarization are likely very minor, suggest that the magnetic field geometry in NGC 891 is predominantly parallel to the plane, on the large scale. The orientation of visible and near-infrared polarization vectors in NGC 891 suggest, however, a vertical magnetic field if the polarization is due to aligned grains (Scarrott & Draper 1996; Wood & Jones 1997). Again, this discrepancy may be due to the differing resolutions of the two datasets or to optical depth effects in the optical/IR region.

The presence of magnetic fields, particularly parallel to the plane, may significantly affect the processes that cycle material between the disks and halos of spiral galaxies, though we have thus far neglected the role of magnetic fields in our discussion. The addition of magnetic pressure in the calculated evolution of SNRs generally leads to smaller remnants, at least in the direction perpendicular to the local magnetic fields (cf., Slavin & Cox 1992). Magnetic fields oriented parallel to the plane of a spiral galaxy provide a tension that could confine the  $z$ -expansion of superbubbles. This tension makes it more difficult for large superbubbles to break out of the thin interstellar disk of a galaxy; all of which would seem to suggest that the presence of magnetic fields might quench disk-halo circulation in disk galaxies if of sufficient strength and the correct orientation.

On the other hand, a configuration wherein horizontal magnetic fields provide partial support against a vertical gravitational field is subject to the Parker instability (Parker 1966). As a supershell or other disturbance pushes the field upward in a small region, matter slides down the field lines, which reduces the weight providing confinement of the magnetic field. The field continues its expansion to higher  $z$ , given that less material is holding it down, forming an  $\Omega$ -shaped structure as matter continues to slide down the now-vertical sides of the magnetic arch. This process, known as the Parker instability, may play an important role in the dynamics of interstellar material (Basu et al. 1997; Matsumoto et al. 1990). Though magnetic fields are generally thought to impede the blow-out of superbubbles into the halo, the existence of a Parker-unstable region of a spiral may in fact aid in the lifting of material beyond the thin disk (Kamaya et al. 1996). The Parker instability may be excited variously by supernovae-driven phenomena (Kamaya et al. 1996) or by inflation of relativistically hot cosmic-ray gas (Parker 1992).

Indeed, a subset of the absorbing structures seen in NGC 891 is reminiscent of magnetically shaped phenomena. Further, the Parker instability predicts that matter will flow down the sides of the arched magnetic field. The material that has fallen down either side of the field structure will appear as a vertically-oriented “column.” Structures such as feature 4 could represent the end result of this type of magnetic field evolution.

The orientation of the magnetic field could also significantly affect the expulsion of dusty material via radiation pressure from galactic starlight. If the magnetic fields are predominantly parallel to the plane of a galaxy, it would seem difficult to radiatively expel grains from the thin disk, assuming the grains are charged and would thus be coupled to the magnetic field. In regions where the magnetic field runs perpendicular to the disk, this would be less significant a problem. Sofue et al. (1994) have suggested that the absorbing structures seen in NGC 253 may be caused by radiation driving along vertical magnetic fields. They argue that magnetic fields should be invoked because of the general morphologies of their features, particularly given the coherency exhibited by their features over lengths of a kpc or more.

Though the radio observations suggest that the large scale field lies generally parallel to the disk, there may be small-scale variations in the magnetic field geometries along which dust could be driven. The fact that vertical fields do not dominate the radio continuum observations suggests, however, that coherent vertically-oriented fields stretching for large distances are not likely; thus it would be difficult to drive grains to the very large  $z$ -heights suggested by the Ferrara et al. (1991) models. However, for the structures apparent in the WIYN images, it may be the case that the local fields run perpendicular for long enough distances to allow radiation pressure expulsion of grains to the requisite heights.

#### 6.4. Ejection via Dynamical Instabilities

It may be possible to lift material from the thin disk via dynamical instabilities. Binney (1981) and Mulder & Hooimeyer (1984) have studied resonant excitation of  $z$ -directed instabilities in the collisionless motions of stars, concluding that stars in flattened potentials may be driven in the  $z$ -direction via resonant coupling of  $z$ -oscillations and changes in the radial component of the force. The coupling requires highly eccentric orbits or non-axisymmetric potentials, i.e., bars. For disk galaxies this coupling occurs in only relatively thin annuli at specific radii. More recently Erwin & Sparke (1997, in preparation) have investigated models of pre-main sequence gaseous circumbinary accretion disks by following the orbits of particles which have a fixed artificial viscosity; they similarly find that material may be excited to highly inclined orbits via dynamical instabilities and resonances.

All of these models rely upon resonances of particle orbits with non-axisymmetric or bar-like potentials to excite the vertical motions. Though there may be evidence for a central bar in NGC 891 (García-Burillo & Guélin 1995), there still exists the problem of energy dissipation in self-

or disk-crossing orbits. These investigations have all studied *collisionless* orbits, while for the present problem of gaseous material, orbits that are self-crossing or disk plane-crossing may lead to significant energy loss and possibly shocks. It has yet to be seen whether gaseous material can fully participate in these trajectories given its collisional nature. It may be the case that parcels of the ISM can be thrown out of the plane of a barred galaxy, but that the trajectory may be significantly altered as it nears the plane by the material's interaction with disk gas. Also the orbits described by Binney (1981) and Mulder & Hooimeyer (1984) rely upon resonance effects which, for a characteristic  $z$ -oscillation frequency, occur in thin annuli at specific distances. Thus if the dust seen away from the plane of NGC 891 were expelled via this type of resonant coupling, we would expect to find no high- $z$  material beyond a cut-off point at some projected distance from the center of the galaxy, which is not seen.

Dynamical instabilities as a whole can probably not be rejected at this time, though it is not clear that they are capable of producing the wide-spread extraplanar dust seen in NGC 891.

### 6.5. Why NGC 891?

It is not the case that all galaxies show an extensive network of extraplanar dust structures like that seen in NGC 891. A counter example to this phenomenon is the Sb galaxy NGC 4565, also at a distance of  $\sim 10$  Mpc; initial WIYN images of this galaxy at  $0.75''$  resolution show a few very localized examples of dust stretching away from the midplane to high  $z$ , but nothing like the pervasive extraplanar dust found in NGC 891.

While it is too early to definitively declare causes for the phenomenon of extraplanar dust in NGC 891, it is important to point out that NGC 891 is not typical of most galaxies in various respects, extraplanar dust structures possibly being one. The radio continuum and  $H\alpha$  halos found in NGC 891 are not common. Hummel et al. (1991), in a search for extended radio continuum halos around edge-on galaxies, found only 10% of the galaxies show any extended- $z$  emission; only 5% of these were thought to be good candidates for the further study of extraplanar emission.

Further, it is becoming increasingly clear that extraplanar  $H\alpha$  emitting material is not common among galaxies, particularly relatively smoothly distributed, wide-spread emission as seen about NGC 891 (Rand 1996; Pildis et al. 1994b; Dettmar 1992). Several galaxies show filamentary extensions (e.g., NGC 5775), while some exhibit a patchy distribution of ionized material (e.g., NGC 4217). The few galaxies that seem to show evidence for smoothly distributed or wide-spread extraplanar DIG generally have relatively high far-infrared luminosities and surface brightnesses, which may indicate that the existence and appearance of extraplanar  $H\alpha$  emission from galaxies depends on the star formation rate or star formation rate per unit area of the underlying disk (Rand 1996). The extraplanar DIG in NGC 891 is significantly brighter than that from most other galaxies.

The ionizing spectrum required to produce the observed emission line ratios from the ionized



halo of NGC 891 is likewise quite extreme, though the only point of comparison currently available is the DIG of the Milky Way. The very deep spectrum of the extraplanar DIG obtained by Rand (1997) suggests that nearly 70% of the He in this diffuse layer may be singly-ionized. This conclusion is based upon the ratio of the He I 5876 Å line to H $\alpha$ ; the input spectrum required to provide this level of ionization is significantly harder than that required by the Reynolds & Tufte (1995) result for DIG in the Milky Way.

If the strength of the extraplanar DIG and radio continuum emission in NGC 891 is indeed related to vigorous star formation in the underlying disk, the spectacular extraplanar dust features seen in our WIYN images may also be a result of the enhanced energy input associated with high levels of star formation. If these dust structures are the result of a very high star formation rate within the disk of NGC 891, they may be shaped by the hydrodynamical afterlives of massive stars or the enhanced radiative driving force on dusty clouds due to the greater number of these stars, or perhaps by the combination of the two mechanisms. We emphasize once again that the potential energies derived in Sect. 4.3 are very much lower limits to the input energies required to lift the observed dust structures from the midplane. In models involving explosively-driven expulsion, the consideration of radiative losses and conversion of kinetic into thermal energy may require as much as an order of magnitude greater energy input in order to lift the clouds to their current positions than those given in Table 3. Thus, if the structures we see in NGC 891 are shaped primarily by the effects of multiple supernovae, the energy input of several thousand such explosions may be required to explain the  $z$ -heights of several of these absorbing features. This is a great deal of energy, though not outside the realm of possibility for the larger OB associations.

Rand (1996) has found that several galaxies show quite localized patches of extraplanar DIG (e.g., NGC 4217 and NGC 5023). If these cases of localized DIG are due to very locally enhanced star formation rate, we might expect to find extraplanar dust filaments only in these regions of the galaxies; for NGC 891, or other galaxies with wide-spread H $\alpha$  emission, there may be high levels of star formation activity throughout the disk, and thus also wide-spread extraplanar dust features, if the dust structures are driven by star formation. The dust features seen in NGC 891 may very well represent extragalactic examples of the dusty “worms” of Koo et al. (1992), particularly as seen in their IRAS 100  $\mu$ m images, or the walls of the “chimneys” postulated by Norman & Ikeuchi (1989). We note that the star formation rate of NGC 4565, which does not show widespread extraplanar dust features, is significantly lower than that of NGC 891 (as traced by the far-infrared luminosity, which is 20% of that found from NGC 891). For now we can only speculate that the existence of the dust structures discussed in this paper *may* be associated with the relatively high star formation rate of NGC 891.

The discussion in Sect. 4.5 regarding pure number counts, while obviously incomplete, shows that  $\sim 2 \times 10^8 M_{\odot}$  of gas may exist well beyond the thin disk of NGC 891. García-Burillo et al. (1992) comment that their extended component of CO emission might have a total mass in the range  $10^8 - 10^9 M_{\odot}$ . While this is not conclusive evidence, there may be a connection between the dust seen in our WIYN images and the high- $z$  CO emission reported by García-Burillo et al.

Also, the dusty features seen here may be connected with high-velocity cloud populations observed in spiral galaxies. Schulman et al. (1994) find several galaxies with high-velocity wings that may represent a population of high-velocity clouds. They derive gas masses for this component in the range  $6 \times 10^7$  to  $4 \times 10^9 M_{\odot}$ , 4-14% of the total estimated H I mass of the galaxies in question. The fractional and total masses of this material are not unlike our estimates for the dust-containing features above the plane of NGC 891, possibly also suggesting a connection between these components.

The masses of individual extraplanar dust features are similar to those of the Galactic giant molecular clouds. Might these dust features be high- $z$  examples of such clouds? If the masses derived here are correct, or lower limits given our neglect of scattering, the possibility exists that star formation may be occurring well away from the plane of NGC 891 in some of these structures. Particularly for the most opaque structures, such as feature 1. A careful search for young extraplanar star clusters and possible associated H $\alpha$  emission will be a goal for our next investigation of NGC 891.

## 7. Summary

We present high-resolution (0.60-0.65") optical BVR images of the edge-on Sb galaxy NGC 891 obtained with the WIYN 3.5-m telescope. The images reveal a wealth of halo absorbing dust structures viewed against the background stellar light of the galaxy. A study of these structures leads us to the following conclusions:

1. The WIYN images reveal hundreds of dust absorption structures in the disk-halo boundary of NGC 891. The structures have a wide range of often complex morphologies and are found up to  $\sim 1.5$  kpc from the mid-plane of the galaxy.

2. The dust features cannot be attributed to a warp because they extend to both sides of the mid-plane of NGC 891. The features are not likely to be associated with a flared gas layer at large galactocentric distances because the WIYN data reveal evidence for foreground stellar light and some of the features appear to be associated with star formation events in the disk. We attribute the dust structures to inner galaxy ( $R < 10$  kpc) high- $z$  features. The dust features provide important information about the processes that eject gas and dust into galaxy halos.

3. Twelve dust structures identified for detailed study are typically hundreds of pc in length and 50 to 100 pc in width. Assuming a Milky Way hydrogen to dust extinction ratio, the inferred total hydrogen column densities in these features range from  $\sim 1$  to  $4 \times 10^{21} \text{ cm}^{-2}$ , and their masses range from  $\sim 2$  to  $50 \times 10^5 M_{\odot}$ . The gravitational potential energies of the dust structures are greater than 20 to  $\sim 200 \times 10^{51}$  ergs. If the high- $z$  dust is expelled from the disk, the input energies may be significantly larger than the observed potential energy. These quantities should be regarded as *lower* limits.

4. The dust structures exhibit a wide range of complicated morphologies. There are round and irregular clouds, vertical columns, loop-like structures, cometary clouds and vertical cones. The higher-resolution HST image discussed herein shows the structures to be filamentary on a scale even finer than that seen in the WIYN images. Some of the observed complexity may be due to overlapping clouds along the line of sight.

5. We estimate at least 120 dust features exist at  $|z| \gtrsim 400$  pc with  $a_B \gtrsim 0.25$  mag. Assuming Galactic gas to dust ratios, the total implied mass of gas associated with these dust structures exceeds  $2 \times 10^8 M_\odot$ , or approximately 2% of the total neutral gas mass of NGC 891. There may be a significantly greater number of structures than our counts suggest due to confusion along the line of sight and our inability to pick out structures deep into the galaxy because of foreground stellar light contamination.

6. Several dust structures are clearly associated with  $H\alpha$  emission structures that extend from regions of very active star formation in the disk towards the halo. The most pronounced examples are bubble- and cone-shaped.

7. The off-plane dust structures have apparent extinction properties best characterized by  $R_V \equiv A_V/E(B - V) \approx 3.6 \pm 0.4$ , where  $R_V$  is the ratio of V-band selective to total extinction. This value is roughly consistent with the typical  $R_V$  for Galactic diffuse clouds.

8. The effects of large amounts of extinction, due to the presence of extensive quantities of dust at large  $z$ -distances from the plane of NGC 891, must be allowed for when attempting to interpret other data relating to off-plane stellar and interstellar emission from NGC 891.

9. The high values of  $N_H$  and large inferred masses for the more prominent halo dust structures raises the possibility that much of the hydrogen in these features is molecular and that some of the clouds may be sites for current or future star formation.

10. We have reviewed a number of expulsion mechanisms that might explain the existence of extraplanar gas and dust in the halos of spiral galaxies. In several cases the dust features we observe have shapes and energy requirements suggestive of ejection phenomena driven by multiple supernova, such as galactic chimney and fountain processes. Others have appearances open to a wide range of possible explanations.

11. The processes that lift gas and dust into galaxy halos evidently are not violent enough to completely destroy the dust grains. Important non-destructive processes worthy of detailed study include low-temperature galactic fountains, the radiative expulsion of grains and various magnetic and dynamical processes.

JCH recognizes the guidance of Drs. G.D. Nickas, D.L. Steinert and H.S. Thompson. We also owe thanks to J. Gallagher, J. Mathis and A. Ferrara for their comments and suggestions, as well as C. Corson, D. Sawyer and T. von Hippel for their expert help with technical issues. We appreciate the help of A. Cole in dealing with the WFPC2 filter extinction characteristics.

Special thanks goes to Dr. N. Sharp of NOAO for producing the true color image shown here as Figure 1. We thank the anonymous referee for a careful reading of this text and for making valuable suggestions on its improvement. Our deep appreciation is extended to the many people who had significant roles in the planning and construction of the WIYN Observatory and in the optimization of the scientific performance of the telescope. We also acknowledge the major support from the higher administration of the University of Wisconsin-Madison which made possible our department's participation in the WIYN Observatory project. JCH and BDS acknowledge support from NASA grant NAG5-1852.

### REFERENCES

- Aoki, T.E., Hiromoto, N., Takami, H. & Okamura, S. 1991, PASJ, 43, 755
- Bahcall, J.N. 1984, ApJ, 276, 169
- Basu, S., Mouschovias, T.Ch. & Paleologou, E.V. 1997, ApJ, 480, 55
- Binney, J. 1981, MNRAS, 196, 455
- Bohlin, R.C., Savage, B.D. & Drake, J.F. 1978, ApJ, 224, 132
- Bregman, J.N. 1980, ApJ, 236, 577
- Bregman, J.N. 1997, ApJ, in press
- Bregman, J.N. & Pildis, R.A. 1994, ApJ, 420, 570
- Cardelli, J.A., Clayton, G.C. & Mathis, J.S. 1989, ApJ, 345, 245
- Cioffi, D.F. 1986, in NRAO workshop No. 12, Gaseous Halos of Galaxies, eds. J.N. Bregman & F.J. Lockman, (NRAO), p. 235
- Cole, A.A., Gallagher, J.S., Freedman, W.L. & Phelps, R. 1997, AJ, 113, 1700
- Dahlem, M., Dettmar, R.-J. & Hummel, E. 1994, A&A, 290, 384
- Dettmar, R.-J. 1990, A&A, 232, L15
- Dettmar, R.-J. 1992, Fund. Cosm. Phys., 15, 141
- Dickey, J.M. & Lockman, F.J. 1990, ARA&A, 28, 215
- Dumke, M., Krause, M., Wielebindki, R. & Klein, U. 1995, A&A, 302, 691
- Elmegreen, D.M. 1980, ApJS, 43, 37
- Fendt, C., Beck, R., Lesch, H. & Neininger, N. 1996, A&A, 308, 713
- Ferrara, A. 1993, ApJ, 407, 157
- Ferrara, A. 1997, in The Physics of Galactic Halos, in press.
- Ferrara, A., Ferrini, F., Barsella, B. & Franco, J. 1991, ApJ, 381, 137
- Franco, J., Ferrini, F., Barsella, B., & Ferrara, A. 1991, ApJ, 366, 443

- Gallagher, J.S. & Hunter, D.A. 1981, *AJ*, 86, 1312
- García-Burillo, S., Guélin, M., Cernicharo, J. & Dahlem, M. 1992, *A&A*, 266, 21
- García-Burillo, S. & Guélin, M. 1995, *A&A*, 299, 657
- Greenhouse, M.A., Woodward, C.E., Thronson, H.A., Rudy, R.J., Rossano, G.S., Erwin, P. & Puetter, R.C. 1991, *ApJ*, 383, 164
- Guélin, M., Zylka, R., Mezger, P.G., Haslam, C.G.T., Kreysa, E., Lemke, R. & Sievers, A.W. 1993, *A&A*, 279, L37
- Handa, T., Sofue, Y., Ikeuchi, S., Kawabe, R. & Ishizuki, S. 1992, *PASJ*, 44, L227
- Heiles, C. 1979, *ApJ*, 229, 533
- Heiles, C. 1984, *ApJS*, 55, 585
- Houck, J.C. & Bregman, J.N. 1990, *ApJ*, 352, 506
- Hummel, E., Beck, R. & Dettmar, R.-J. 1991, *A&AS*, 87, 309
- Jones, A.P., Tielens, A.G.G.M., Hollenbach, D.J. & McKee, C.F. 1994, *ApJ*, 433, 797
- Jones, T.J. 1997, *AJ*, submitted.
- Kamaya, H., Mineshige, S., Shibata, K. & Matsumoto, R. 1996, *ApJ*, 458, L25
- Keppel, J.W., Dettmar, R.-J., Gallagher, J.S. & Roberts, M.S. 1991, *ApJ*, 374, 507
- Knapen, J.H., Hes, R., Beckman, J.E. & Peletier, R.F. 1991, *A&A*, 241, 42
- Koo, B.-C., Heiles, C. & Reach, W.T. 1992, *ApJ*, 390, 108
- Kovalenko, I.G. & Levy, V.V. 1992, *A&A*, 264, 406
- Kuijken, K. & Gilmore, G. 1989, *MNRAS*, 239, 605
- Kurucz, R.L. 1991, in *Precisioin Photometry: Astrophysics of the Galaxy*, eds. A.G.D. Philip, A.R. Upgren and K.A. Janes (Davis, Schenectady), p. 27
- Kylafis, N.D. & Bahcall, J.N. 1987, *ApJ*, 317, 637
- Lockman, F.J. 1984, *ApJ*, 283, 90
- Martos, M., Moreno, E. & Cox, D. *BAAS*, 188, 4311
- Matsumoto, R., Horiuchi, T., Hanawa, T. & Shibata, K. 1990, *ApJ*, 356, 259
- Mihalas, D. & Binney, J. 1981, *Galactic Astronomy*, 2nd ed., (Freeman)
- Morrison, H.L., Miller, E.D., Harding, P., Stinebring, D.R. & Boroson, T.A. 1997, *AJ*, 113, 2061
- Mulder, W.A. & Hooimeyer, J.R.A. 1984, *A&A*, 134, 158
- Norman, C.A. & Ikeuchi, S. 1989, *ApJ*, 345, 372
- Parker, E.N. 1966, *ApJ*, 145, 811
- Parker, E.N. 1992, *ApJ*, 401, 137

- Pildis, R.A., Bregman, J.N. & Schombert, J.M. 1994a, ApJ, 423, 190
- Pildis, R.A., Bregman, J.N. & Schombert, J.M. 1994b, ApJ, 427, 160
- Rand, R.J. 1996, ApJ, 462, 712
- Rand, R.J. 1997, ApJ, 474, 129
- Rand, R.J., Kulkarni, S.R. & Hester, J.J. 1990, ApJ, 352, 1
- Reynolds, R.J. & Tufte, S.L. 1995, ApJ, 439, 17
- Rupen, M. 1991, AJ, 102, 48
- Sancisi, R. & Allen, R.J. 1979, A&A, 74, 73
- Savage, B.D., Drake, J.F., Budich, W. & Bohlin, R.C. 1977, ApJ, 216, 291
- Savage, B.D. & Mathis, J.S. 1979, ARA&A, 17, 73
- Sembach, K.R. & Savage, B.D. 1996, ApJ, 457, 211
- Scarrott, S.M. & Draper, P.W. 1996, MNRAS, 278, 519
- Schulman, E., Bregman, J.N. & Roberts, M.S. 1994, ApJ, 423, 180
- Scoville, N.Z., Thakkar, D., Carlstrom, J.E. & Sargent, A.I. 1993, ApJ, 404, L59
- Seaton, M.J. 1979, MNRAS, 187, 73
- Shapiro, P. & Field, G.B. 1976, ApJ, 205, 762
- Slavin, J.D. & Cox, D.P. 1992, ApJ, 392, 131
- Sofue, Y. 1987, PASJ, 39, 547
- Sofue, Y., Wakamatsu, K-I. & Malin, D. 1994, AJ, 108, 2102
- Suchkov, A.A. & Shchekinov, I.U.A., 1975, Astrophysics, 10, 159
- Sukumar, S. & Allen, R.J. 1991, ApJ, 382, 100
- Swaters, R., Sancisi, R. & van der Hulst, J.M. 1995, Astro. Lett. and Communications, 31, 161
- Swaters, R.A., Sancisi, R. & van der Hulst, J.M. 1997, ApJ, in press
- van der Hulst, J.M. 1996, in The Minnesota Lectures on Extragalactic Neutral Hydrogen, ed. E.D. Skillman (PASP), p. 47
- van der Kruit, P.C. 1988, A&A, 192, 117
- van der Kruit, P.C. & Searle, L. 1981, A&A, 95, 116
- Wainscoat, R.J., de Jong, T. & Wesselius, P.R. 1987, A&A, 181, 225
- Wakker, B., Howk, C., Schwarz, U., van Woerden, H., Beers, T., Wilhelm, R., Kalberla, P. & Danly, L. 1996, ApJ, 473, 834
- Wood, K. & Jones, T.J. 1997, AJ, submitted.

Fig. 1.— A three-color (BVR) image of NGC 891 as seen with the full  $6.7' \times 6.7'$  field of the WIYN CCD. In this image North is  $20^\circ$  clockwise from the top and East is similarly angled from the left edge. The seeing limited resolutions of the individual BVR images are  $0.60''$ - $0.65''$ . The resolution of this three color composite image is slightly worse. Note the presence of large numbers of absorbing dust far from the mid-plane of the galaxy. (We thank Dr. N. Sharp of NOAO for processing this image.)

Fig. 2.— A B-band view of NGC 891; this figure has a resolution of  $0.65''$ , slightly better than that of Figure 1. North and East are indicated on this figure; the bar in the lower left corner of the image represents 1 kpc at a distance of 9.5 Mpc. Again, numerous filamentary dust structures are seen far from the thin disk of NGC 891, some at heights of at least 1.5 kpc from the mid-plane.

Fig. 3.— (a) A B-band close-up of the central bulge of NGC 891 with  $0.65''$  seeing and (b) an unsharp-masked version of this same region. The region displayed covers  $2.2' \times 1.5'$ . The scale of the image is given in kpc on the side and bottom of the figure, referring to the  $z$ -height and projected radial distance from the center, respectively. Some stars have been removed in producing the unsharp-masked image.

Fig. 4.— As Figure 3(a) and (b), but for a section of the disk to the NE of the bulge. This section is  $\sim 5$  kpc from the center of the galaxy. This is a region of very active star-formation and shows dust structures extending to high- $z$  that are likely caused by the effects of multiple supernovae.

Fig. 5.— As Figure 3(a) and (b), but for a section of the disk to the SW of the bulge. This section is  $\sim 5$  kpc from the center of the galaxy and seems to have a significantly lower star-formation rate than the region shown in Figure 4. Several stars that lay directly on the disk or in the low halo that have been removed can be seen in the unsharp-masked version of this image.



Fig. 6.— Apparent extinction for B- and R-bands (squares and triangles, respectively) versus that in V-band for high- $z$  dust in NGC 891. The solid lines represent the Galactic relationship which would hold if the dust structures were all on the front side of the galaxy with  $R_V=3.6$ . The dotted lines are the values expected for the apparent extinction in the B- and R-bands if the clouds have a fraction  $x$  of the stellar light in front of them. The numbers on the plot give the values of  $x$ . Also plotted as dashed lines are the expected behaviors for clouds characterized by  $R_V=3.2$  and 4.0 (outer and inner dashed lines, respectively). These values are the  $1\sigma$  deviations from the best fit to the data. The cross in the lower right shows the approximate  $\pm 1\sigma$  error bars for the data points.

Fig. 7.— (a) A B-band close-up of the section to the NE of the bulge [same as 4(a)] and (b) an image of ionized gas in this region ( $H\alpha+[N II]$ ). A comparison of the B-band and ionized gas images show correspondences between structures seen in dust absorption and ionized gas. It should be noted that this image is inverted across the horizontal axis from that shown in Pildis et al. (1994).

Fig. 8.— The 180-s F606W WFPC2 image of the central region of NGC 891 at  $0.10''$  resolution. This figure should be compared with the WIYN image of a similar region given in Figure 3, though the WIYN image shown in that figure was obtained in the B-band.

Fig. 9.— Close-ups of features 1 and 2 as seen by WIYN and HST (left and right, respectively). The WIYN close-up is from the B-band image, while the HST image was taken through the F606W filter. The region displayed is  $30''$ , or  $\approx 1.3$  kpc, on a side. Though the B-band image is more sensitive to low apparent extinction features, the differences in resolution are shown clearly.

Fig. 10.— As for Figure 9, but centered on feature 4, also showing features 3. Again, the region displayed is  $30''$ , or  $\approx 1.3$  kpc, on a side.

Table 1. Observing Log

Filter	Exposure (sec.)	Pix. Scale (arcsec pix <sup>-1</sup> )	Resolution (arcsec)	Resolution (pc)
WIYN Images				
B	500	0.196	0.65	30
V	120	0.196	0.65	30
R	300	0.196	0.60	28
H $\alpha$	2100	0.196	0.90	41
HST WFPC2 Images				
F606W	2 $\times$ 90	0.1	0.1 <sup>a</sup>	5 <sup>a</sup>

<sup>a</sup>The HST PSF is undersampled in the WFC CCD.

Table 2. Observed Properties of Selected Dust Features

Feature	R.A. <sup>a</sup> (B1950.0)	Dec. <sup>a</sup> (B1950.0)	Length <sup>b</sup> (pc)	Width <sup>c</sup> (pc)	$z^d$ (pc)	$a_B^e$	$a_V^e$	$a_R^e$	Morphology <sup>f</sup>
1	2 <sup>h</sup> 19 <sup>m</sup> 22.0 <sup>s</sup>	42° 06′ 40″	360	~300	≲ 800	1.55	1.31	1.05	Vert. column
2	2 19 20.4	42 06 44	100	50	1450	0.84	0.65	0.54	Elongated cloud
3	2 19 22.6	42 07 21	210	90	1120	0.45	0.37	0.31	Irr. cloud
4	2 19 23.8	42 07 36	450	75	≲ 1350	1.11	0.80	0.65	Vert. column
5	2 19 25.6	42 06 49	145	45	950	0.59	0.49	0.37	Irr. cloud
6	2 19 25.4	42 06 56	250	90	700	0.75	0.65	0.47	Irr. cloud
7	2 19 26.5	42 06 51	110	60	1350	0.37	0.30	0.24	Cometary cloud?
8	2 19 26.1	42 07 23	360	70	≲ 750	0.59	0.52	0.36	Vert. column
9	2 19 27.2	42 07 46	400	350	≲ 1000	0.61	0.50	0.40	Vert. column
10	2 19 29.4	42 08 47	600	270	≲ 900	0.59	0.52	0.36	Vert. cone
11a	2 19 30.2	42 09 01	250	65	≲ 750	0.80	0.59	0.50:	Shell wall
11b	2 19 30.7	42 09 13	250	55	≲ 800	0.40	0.39	0.30:	Shell wall
12	2 19 26.9	42 09 00	600:	80	≲ 1000	1.00	0.82	0.67	Irr. vert. column

<sup>a</sup>Approximate coordinates of the dust feature.

<sup>b</sup>Long dimension in parsecs.

<sup>c</sup>Short dimension in parsecs.

<sup>d</sup>Height above the midplane, or the limit to which very extended features can be traced.

<sup>e</sup>Apparent extinction for the BVR wavebands in magnitudes, as defined in the text.

<sup>f</sup>Morphological description; these are very subjective.

Table 3. Derived Properties of Selected Dust Features

Feature	$A_V^a$	$N_H^b$ ( $10^{20} \text{ cm}^{-2}$ )	$x^c$	Mass <sup>d</sup> ( $10^5 M_\odot$ )	Energy <sup>e</sup> ( $10^{51}$ ergs)
1	1.79	30	0.1	40	130
2	0.79	13	0.1	2	25
3	0.94	16	0.5	5	45
4	0.71	12	0	8	40
5	0.73	12	0.3	3	24
6	1.00	17	0.3	5	20
7	0.66	11	0.5	2	30
8	0.80	13	0	5	20
9	0.90	15	0.4	20	80
10	0.85	14	0.3	20	70
11a	0.63:	10:	0:	10:	50:
11b	1.96:	32:	0.7:	50:	240:
12	1.26	21	0.2	20	120

<sup>a</sup>Value derived for the V-band extinction (in magnitudes) using equation (2) in three colors and assuming  $R_V \approx 3.5$ . These estimates neglect the fact that starlight is scattered into the beam (see Sect. 4.2).

<sup>b</sup>Approximate column density of material (in units of  $10^{20} \text{ cm}^{-2}$ ) assuming Galactic extinction and gas-to-dust conversions.

<sup>c</sup>Fraction of stellar light coming from in front of the absorbing feature derived using equation (2) in three colors. This quantity is to be considered highly uncertain, particularly given our neglect of scattered light (see Sect. 4.2).

<sup>d</sup>Approximate mass based upon column density and projected area (given in units of  $10^5 M_\odot$ ).

<sup>e</sup>Approximate potential energy of the observed material given its mass and height from the midplane (in units of  $10^{51}$  ergs, the approximate energy imparted to the ISM from a single supernova).

This figure "n891.fig1.jpg" is available in "jpg" format from:

<http://arxiv.org/ps/astro-ph/9709197v1>

This figure "n891.fig2.jpg" is available in "jpg" format from:

<http://arxiv.org/ps/astro-ph/9709197v1>

This figure "n891.fig3.jpg" is available in "jpg" format from:

<http://arxiv.org/ps/astro-ph/9709197v1>

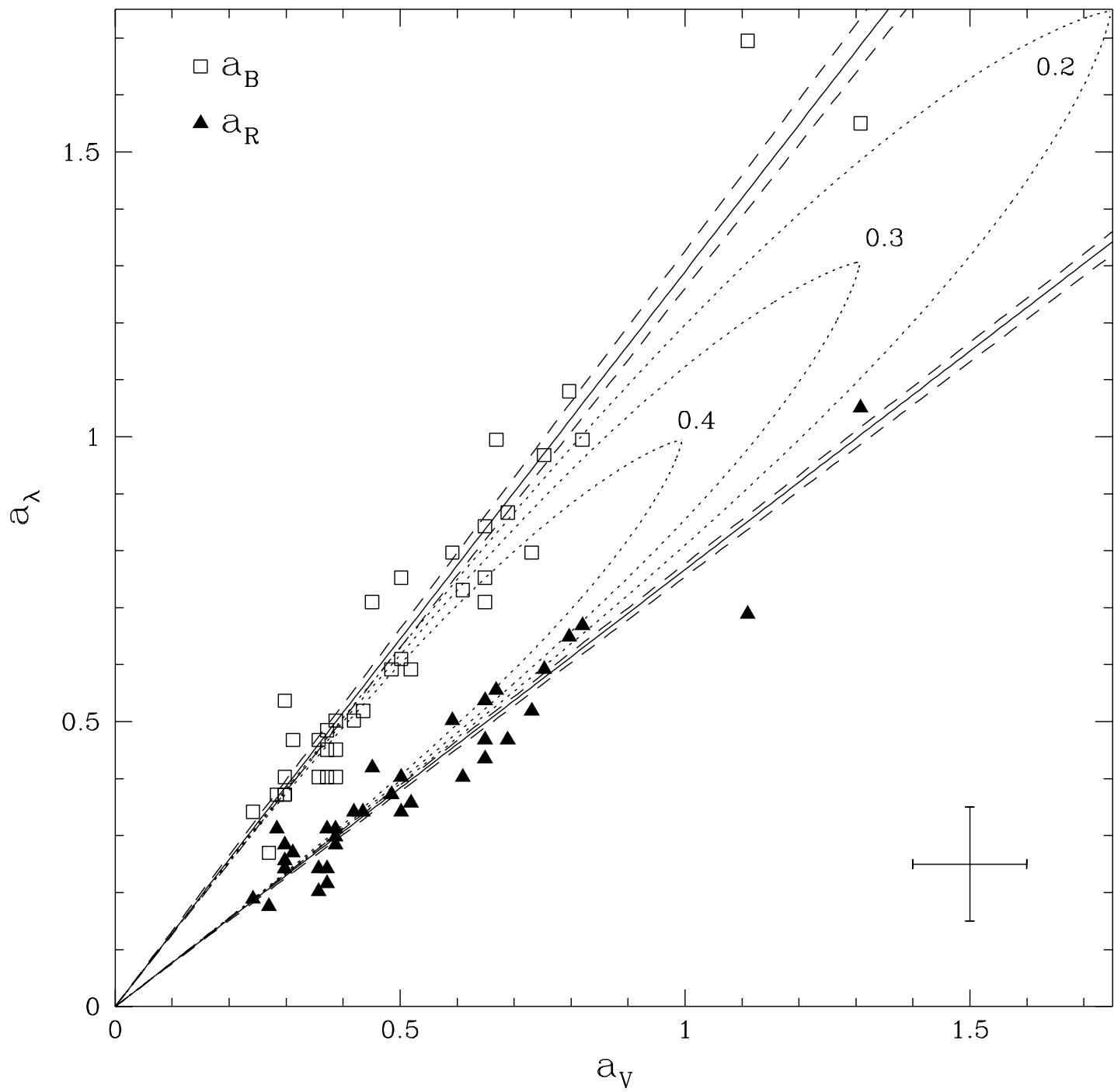


This figure "n891.fig4.jpg" is available in "jpg" format from:

<http://arxiv.org/ps/astro-ph/9709197v1>

This figure "n891.fig5.jpg" is available in "jpg" format from:

<http://arxiv.org/ps/astro-ph/9709197v1>



This figure "n891.fig7.jpg" is available in "jpg" format from:

<http://arxiv.org/ps/astro-ph/9709197v1>

This figure "n891.fig8.jpg" is available in "jpg" format from:

<http://arxiv.org/ps/astro-ph/9709197v1>

This figure "n891.figs9\_10.jpg" is available in "jpg" format from:

<http://arxiv.org/ps/astro-ph/9709197v1>